# Optimal Drag-Energy Entry Guidance via Pseudospectral Convex Optimization

Marco Sagliano *

*German Aerospace Center, Bremen, 28359, Germany*

Erwin Mooij †

*Delft University of Technology, Delft, The Netherlands, 2629*

**In this paper a new drag-energy scheme, based on the use of pseudospectral methods and convex optimization, is proposed. One of the most successful technologies to deal with atmospheric entry is the class of drag-tracking schemes, a direct heritage of the Space Shuttle program. The method that we propose exploits the drag-dynamics, and allows for an efficient automatic design of an optimal entry profile satisfying all the longitudinal constraints acting on the vehicle. A new representation of the entry-guidance problem, able to loss-less convexify the formulation, is provided. Numerical simulations confirm the validity of the proposed scheme as tool for further improving the autonomy of modern entry guidance systems, with a mean final range-to-go error in the order of three hundred meters, and the capability to re-compute a complete constrained trajectory to meet the mission requirements.**

## I. Introduction

Since the beginning of the Apollo program, entry guidance has been widely treated by engineers and researchers. The first, successful approach, used for several programs (Apollo, Space Transportation System[1]), was based on the planning of an entry trajectory in terms of the drag-velocity plane. The rationale for this choice resides in the fact that the typical environmental constraints (dynamic pressure, heat flux and load factor), as well as the range-to-go, can be efficiently represented in the drag-velocity plane. The longitudinal guidance can then be derived in several ways. For instance, assuming the equilibrium-glide approximation,[2] extracting the longitudinal states (altitude, speed, flight-path angle) from the drag acceleration and its derivatives,[3] or implementing constraints-tracking guidance schemes.[4] Similar results can be obtained if the drag-velocity plane is replaced by the drag-energy representation.[5–7] In any case, approximations, disturbances and modeling errors make use of a feedback controller necessary to track the scheduled nominal drag profile.

In addition, a bank-reversal logic is usually implemented to keep the heading error within prescribed limits, chosen to steer the vehicle towards the terminal area for energy management (TAEM). In parallel to these approaches, the use of techniques based on optimal control[8–12] has achieved significant improvements. The increased CPU capabilities, together with the development of dedicated algorithms, have led to the possibility to transcribe the problem into a discrete, finite-dimensions problem (i.e., a nonlinear programming problem), which can be efficiently solved with one of the available well-known NLP solvers.[13,14] However, it is in general not possible to define an analytical upper bound for the computational time required to obtain a solution, making the use of these techniques in real-time hard.

Significant steps to relax the CPU burden for inflight application can be found in the use of interpolation-based techniques. Saraf et al.[15] used interpolation schemes applied to extremal drag-energy profiles for generating landing footprints for entry missions. Schierman et al.[16] implemented a scheme able to compute a trajectory online by using piecewise-linear functions, and solved the online trajectory-generation problem as

*Research Engineer, GNC Department, Robert Hooke Str. 7, AIAA Member

†Assistant Professor, Astrodynamics and Space Missions Department, Faculty of Aerospace Engineering, AIAA Associate Fellow

a linear programming problem. Sagliano et al.[17] proposed a multivariate pseudospectral approach to provide a real-time capable method able to deal with large off-nominal conditions. Although properly working, the method only provides sub-optimal solutions, as the optimization is replaced by a multivariate interpolation in between optimal solutions.

The development of convex optimization[18] over the last thirty years boosted the research aiming at solving optimization problems in real-time, since it is possible to predict an upper bound for the number of operations required to solve the problem. This new technology was successfully applied to the powered descent and landing problem by using the so-called *lossless convexification* introduced by Acikmese et al.[19] and further improved over the years.[20] The underlying guidance scheme was then merged with pseudospectral optimal control framework[21] to improve the accuracy of the results.

The application of the hybrid pseudospectral convex optimization gave the hint to revisit the drag-energy schemes previously mentioned. In fact, the drag dynamics and the longitudinal constraints can be reformulated as a convex problem, and discretized according to the pseudospectral convex framework to provide real-time capable drag-energy solutions satisfying all the requirements for a high-performance atmospheric entry. The contribution of this paper are the following: first, a generalized drag-energy dynamics, containing terms usually neglected, are derived. The extended drag-energy scheme is used to formulate the entry-guidance problem in convex form. This is done by using some of the features, such as the differential and the integral operators, coming from pseudospectral methods, specifically, the Lobatto Pseudospectral Method (LPM).[22]

The remainder of this work is organized as follows. Sections II and III provide a brief overview on pseudospectral methods and convex optimization, respectively. The atmospheric entry problem is described in Sec. IV, and applied to HORUS, a winged entry vehicle studied by MBB.[23] The drag-dynamics is the subject of Sec. V, whilst Sec. VI describes the proposed convexification for the drag-energy guidance problem. Section VII demonstrates the performance of the proposed method. Finally, some conclusions are drawn in Sec. VIII.

## II. Pseudospectral methods

### A. Optimal Control Problem

There are several approaches for the generation of reference trajectories. Some methods exploit the structure of the specific problem we deal with. Often, they require simplifications to make the problem mathematically tractable, and therefore generate solutions valid under given hypotheses. A different approach, which nowadays has become a standard method, and benefits from the development of the computational capabilities of modern CPUs, is the representation of the trajectory generation problem as an optimal-control problem. This means that we are looking for solutions minimizing (or maximizing) a given criterion, and satisfying at the same time several constraints, which can be differential (i.e., the equations of motion of a spacecraft) and / or algebraic (e.g., the maximum heat-flux that a vehicle can tolerate during entry). The standard form for representing optimal-control problems is the so-called Bolza problem. Given a state vector $\mathbf{x}(t) \in \mathbb{R}^{n_s}$, a control vector $\mathbf{u}(t) \in \mathbb{R}^{n_c}$, the scalar functions $\Phi(t, \mathbf{x}, \mathbf{u})$ and $\Psi(t, \mathbf{x}, \mathbf{u})$, and the vector $\mathbf{g}(t, \mathbf{x}, \mathbf{u}) \in \mathbb{R}^{n_g}$ we can formulate the problem as follows:

$$\text{minimize} \quad J = \Phi\left[t_f, \mathbf{x}\left(t_f\right), \mathbf{u}\left(t_f\right)\right] + \int_{t_0}^{t_f} \Psi\left[\mathbf{x}(t), \mathbf{u}(t)\right] dt \tag{1}$$

subject to the differential equations

$$\dot{\mathbf{x}} = \mathbf{f}\left(t, \mathbf{x}, \mathbf{u}\right) \tag{2}$$

and to the path constraints

$$\mathbf{g}_L \leq \mathbf{g}\left(t, \mathbf{x}, \mathbf{u}\right) \leq \mathbf{g}_U \tag{3}$$

We also assume that $\mathbf{x}(t)$ and $\mathbf{u}(t)$ are compact in $\mathbb{R}^{n_s}$ and $\mathbb{R}^{n_c}$, respectively:

$$\mathbf{x}_L \leq \mathbf{x}(t) \leq \mathbf{x}_U \tag{4}$$

$$\mathbf{u}_L \leq \mathbf{u}(t) \leq \mathbf{u}_U \tag{5}$$

Moreover, initial and final conditions might be constrained as well.

$$\mathbf{x}_0 = \mathbf{x}(t_0) \tag{6}$$

$$\mathbf{x}_f = \mathbf{x}(t_f) \tag{7}$$

Equations (1)-(7) represent a generic continuous optimal control problem. In the next section we will see how this type of Optimal-Control Problem (OCP) can be transcribed by using pseudospectral methods.

### B. Properties of Pseudospectral Methods

Numerical methods for solving OCPs are divided into two major classes, namely, indirect methods and direct methods. Indirect methods are based on the Pontryagin's Maximum Principle, which leads to a multiple-point boundary-value problem. Direct methods, instead, consist in the proper discretization of the OCP (or *transcription*), having as a result a finite-dimensional NLP problem. Pseudospectral methods represent a particular area of interest in the frame of the wider class of direct methods. Examples of tools implementing pseudospectral methods include DIDO,[24] GPOPS[25] and SPARTAN.[12] For pseudospectral methods the following properties are valid:

- "Spectral" (i.e., quasi-exponential) convergence of the NLP solution to the OCP solution when the number of nodes employed is increased (and the problem is smooth)
- Runge phenomenon is avoided
- Sparse structure of the associated NLP problem

The transcription process does not only involve the choice of the discrete nodes, but also determines the discrete differential and integral operators needed to solve the associated OCP. Therefore, *transcription* is a more general process than *discretization*. The minimum fundamental steps of a *transcription* are the following:

- domain discretization
- discrete to continuous conversion of states and / or controls
- characterization of differential and integral operators

Among the families of pseudospectral (PS) methods a specific one was considered for this work: the Lobatto Pseudospectral Method (or LPM). It is worth saying that this is not the only possible choice, as other sets of nodes, like Gauss,[22] Chebyshev[26] or Radau[12,27] exist. Lobatto pseudospectral method shows good performance, and at the same time allows straightforward computation of initial and final controls, since all the nodes are *collocated*.[27] Therefore, it is useful to have a look at this method.

### C. Lobatto Pseudospectral Method

LPM is based on a symmetric set of nodes, associated with the $n+1$ roots of the Legendre-Lobatto polynomial, defined as

$$L_{n+1}(\tau) = (1-\tau^2)\dot{\tilde{L}}_n \quad \tau \in [-1,1] \tag{8}$$

where $\dot{\tilde{L}}_n$ is the derivative of the Legendre polynomial of order $n$. The roots of the Legendre-Lobatto polynomial and the corresponding polynomial of order 10 are represented in Fig. 1(a). This discrete representation of the domain is useful to reconstruct continuous approximations of the functions $x(t)$ as:

$$\mathbf{x}(t) \cong \sum_{i=0}^{n} \mathbf{X}_i P_i(t), \qquad P_i(t) = \prod_{\substack{k=0 \\ k\neq i}}^{n} \frac{t-t_k}{t_i-t_k} \tag{9}$$

An example of the approximation obtained by means of Eq.(9) is depicted in Fig. 1(b), where the function $1/(1+25\tau^2)$ is reconstructed by using 25 LPM points. It is possible to see that the original function is approximated very well with this set of discrete nodes.

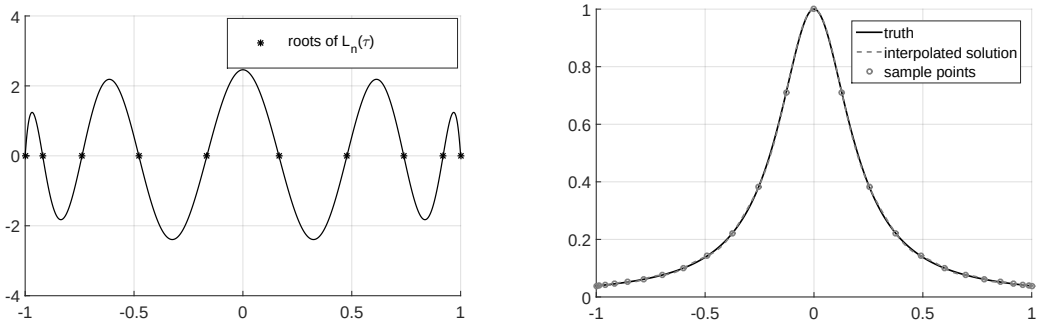


(a) LPM discrete domain

(b) LPM continuous approximation of a function

**Figure 1. Transcription steps for LPM: (a) domain discretization and (b) continuous reconstruction of functions.**

**Remark 1** Note that the approximation becomes more accurate when the number of nodes is increased. This is the opposite behavior observed when uniform distributions of nodes, which suffer from the aforementioned *Runge Phenomenon*, are employed.

Once that the domain has been discretized, and the discrete-to-continuous conversion of states has been defined, the corresponding differential operator needs to be defined. This is required for the proper representation of the left-hand side of Eq. (2). The differential operator will be in the form

$$\dot{\mathbf{X}} \cong \mathbf{D}^1_{Lb} \cdot \mathbf{X} \tag{10}$$

and the dynamics defined in Eq. (2) will be replaced by

$$\mathbf{D}^1_{Lb} \cdot \mathbf{X} = \frac{t_f - t_0}{2} \mathbf{f}(t, \mathbf{X}, \mathbf{U}) \tag{11}$$

where $t_0$ and $t_f$ are the initial and final time, and the term $\frac{t_f - t_0}{2}$ is a scale factor related to the transformation between the physical time domain $t$, and the pseudospectral time domain $\tau \in [-1, 1]$, given by the following affine transformations:

$$t = \frac{t_f - t_0}{2} \tau + \frac{t_f + t_0}{2} \tag{12}$$

$$\tau = \frac{2}{t_f - t_0} t - \frac{t_f + t_0}{t_f - t_0} \tag{13}$$

It is moreover possible to map any domain with respect to the pseudospectral time, by simply changing $t_0$ and $t_f$ with the initial and final values of the new variable, like the energy. The matrix $\mathbf{D}^1_{Lb}$ has dimensions equal to $[n + 1 \times n + 1]$. The initial and final states, together with the corresponding controls, can be determined by the optimization process. However, since the initial state is generally known, further constraints need to be imposed to make sure that the solution found by the optimizer satisfies the condition $\mathbf{x}(t_0) = \mathbf{x}_0$. We can also compute a matrix $\mathbf{D}^2_{Lb}$, which represents the discrete linear operator to compute the second derivative, that is

$$\ddot{\mathbf{X}} \cong \mathbf{D}^2_{Lb} \cdot \mathbf{X} \tag{14}$$

This definition is useful for imposing constraints on the second derivative of a function as linear operator.

If we look at Eq. (9) and we take the derivative w.r.t. time, we get

$$\dot{\mathbf{x}}(t) \cong \frac{d}{dt} \sum_{i=0}^{n} \mathbf{X_i} P(t) = \sum_{i=0}^{n} \mathbf{X_i} \frac{d}{dt} P_i(t) \tag{15}$$

as the nodal points are time-independent. These derivatives can be efficiently computed with the Barycentric Lagrange Interpolation.[28] In addition to the differential operator, we need an integral operator. This operator

is required as the cost function in Eq. (1) may contain the Lagrange term, which needs a proper discretization. In that case the Gauss quadrature formula is used.[29] For the LPM the approach consists of replacing the continuous integral with the discrete sum given by:

$$\int_{t_0}^{t_f} \Psi\left[t, \mathbf{x}(t), \mathbf{u}(t)\right] dt \cong \frac{t_f - t_0}{2} \sum_{i=0}^{n} w_i \Psi\left[\mathbf{X}_i, \mathbf{U}_i\right] \tag{16}$$

It can be shown that Eq. (16) yields exact results for polynomials of order at most equal to $2n-3$.[27] Once again, the presence of the term $\frac{t_f - t_0}{2}$ is a consequence of the mapping between pseudospectral and physical time domains described in Eq. (12) and (13). The weights $w_i$ can be computed as

$$w_j = \begin{cases} \dfrac{2}{(n-1)n}, & j = 0 \\ \dfrac{2}{(n-1)nL_{n-1}(\tau_j)^2}, & j = [1, \ldots, n-1] \end{cases} \tag{17}$$

Once that the differential and integral operators have been described, we are ready to summarize the general NLP transcription, which approximates the original OCP as follows:

Minimize (or maximize) the cost function $J$, for $n+1$ nodes, $i = 0, \ldots, n$,

$$J = \Phi\left[\mathbf{X}_f\right] + \frac{t_f - t_0}{2} \sum_{i=0}^{n} w_i \Psi\left[\mathbf{X}_i, \mathbf{U}_i\right] \tag{18}$$

subject to subject to the nonlinear algebraic constraints

$$\mathbf{F}_i = \mathbf{D}^1_{Lb,i} \cdot \mathbf{X} - \frac{t_f - t_0}{2} \mathbf{f}(t_i, \mathbf{X}_i, \mathbf{U}_i) = \mathbf{0} \tag{19}$$

with $\mathbf{D}^1_{Lb,i}$ representing the $\mathrm{i}^{\mathrm{th}}$ row of the differential matrix. Moreover the system is subject to the discrete version of the path constraints.

$$\mathbf{g}_L \leq \mathbf{G}\left(\mathbf{X}_i, \mathbf{U}_i\right) \leq \mathbf{g}_U \tag{20}$$

The discrete states and the controls are bounded, as in the continuous formulation.

$$\begin{aligned} \mathbf{x}_L \leq \mathbf{X}_i \leq \mathbf{x}_U \\ \mathbf{u}_L \leq \mathbf{U}_i \leq \mathbf{u}_U \end{aligned} \tag{21}$$

More details about LPM can be found in the works of Garg[27] and Sagliano.[21]

## III. Convex Optimization

Over the last thirty years several researchers focused on the development of convex optimization theory.[18,30] They demonstrated that for a large class of problems the key-property is not the linearity of the system, but the convexity. In this case, the problem can be solved in real-time, and if the problem is feasible, the computed solution is the global optimum.

### A. Convex programming

In general a convex optimization problem is defined as follows:

$$\text{minimize } J = f_0(x) \tag{22}$$

subject to

$$f_i(x) \leq a_i, \qquad i = 1, \ldots, m \tag{23}$$

where $x \in \mathbb{R}^n$ represents the vector of variables to be determined. The functions $f_i$, with $i = 0, \ldots, m$, are convex functions, which means that they satisfy the following relationship.

$$f_i(\alpha x + \beta y) \leq \alpha f_i(x) + (1-\alpha) f_i(y), \qquad i = 0, \ldots, m, \quad \forall \alpha \in [0,\ 1] \tag{24}$$

The previous expression suggests one of the properties of convex problems, that is, they generalize the notion of linearity of a function, leading to the notion of convexity, which has the equality as special case instead of the inequality in Eq. (24). Further details and exhaustive explanations can be found in the works of Boyd,[18] and Ben Tal and Nemirovski.[30] The following properties characterize convex optimization:

- A large number of problems can be reformulated in convex form
- There are efficient methods to solve convex problems (e.g., primal-dual interior point methods), such that it can be considered more and more a mature technology
- This class of methods does not require an initial guess (a problem which affects many problems when NLP solvers are employed)
- If a solution to the problem exists, it is the global optimum.

While the category of convex optimization is still quite large, and includes several subfields (e.g., Semidefinite programming, Quadratically constrained quadratic programming, and so on), we will instead focus on a specific form of convex optimization, that is, the so-called Second-order Cone Programming (or SOCP). We will briefly describe this specific subclass of methods in the next section, whereas more extensive and rigorous descriptions of the theoretical properties and the potential applications of this technology can be found in literature.[18,30,31]

### B. Second-Order Cone Programming

An interesting subcategory of convex optimization is represented by Second-Order Cone Programming. This definition encloses all the problems which can be formulated as follows:

$$\text{minimize} \quad c_0^T x \tag{25}$$

subject to

$$\begin{aligned} G_i x &\leq h_i, \quad i = 1, \ldots, l \\ A_0 x &= b_0 \\ \|A_i x + b_i\|_2 &\leq c_i^T x + d_i, \quad i = 1, \ldots, p \end{aligned} \tag{26}$$

with $x \in \mathbb{R}^{n \times 1}$ representing the variables to determine, $c_0 \in \mathbb{R}^{n \times 1}$ is the vector defining the cost function, whereas $G_i \in \mathbb{R}^{l_i \times n}$ and $h_l \in \mathbb{R}^{l_i \times 1}$ represent (with $l_i$ that might vary for every $i$) a set of component-wise inequalities. $A_0 \in \mathbb{R}^{m \times n}$ and $b_0 \in \mathbb{R}^{m \times 1}$ describe the linear system of $m$ equations that the solution has to satisfy. The terms $A_i \in \mathbb{R}^{m_i \times n}$, $b_i \in \mathbb{R}^{m_i \times 1}$, $c_i \in \mathbb{R}^{n \times 1}$ and $d_i \in \mathbb{R}$ describe a conic constraint of order $m_i + 1$. These constraints imply that, given the affine transformations

$$\begin{aligned} t &= c_i^T x + d_i \\ y &= A_i x + b_i, \; i = 1, \ldots, p \end{aligned} \tag{27}$$

the solution will always be contained within the volume of each of the $p$ $m_i$-dimensional cones. Among the others, linear programming problems, or quadratically constrained problems can be reformulated as conic programming problems. Moreover, they can efficiently be solved by using primal-dual interior point methods and several solvers, such as ECOS,[32] are available. These aspects make the SOCP technology appealing for several applications.

## IV. Atmospheric Entry - HORUS

This section will introduce the reentry vehicle used for the simulations, HORUS, and will briefly explain its reference mission and aerodynamics, the environment models, controls, as well as the trajectory constraints.

### A. Reference Mission

The relevant mission details of HORUS are shown in Table 1. HORUS's flight starts above the Pacific Ocean and it ends at the runway at Kourou, French Guiana. The trajectory is split into three parts, the

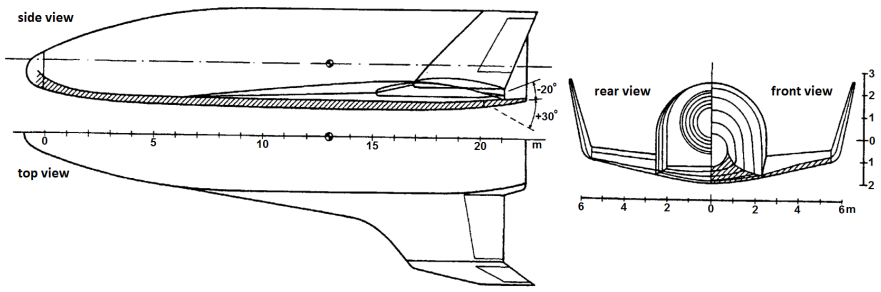


**Figure 2. Different views and the dimensions of HORUS.**[23]

pre-guidance phase, where the aerodynamic forces are too small, and a predefined bank-angle law is used. Once that the vehicle dives deep into the atmosphere, and the aerodynamic accelerations become strong enough to counteract the gravity, the hypersonic guided entry phase begins. This phase nominally begins when 5-10% of the energy is dissipated. Finally, the Terminal Area Energy Management (TAEM) phase before landing comes. To properly protect HORUS during the entry, a predefined angle of attack is defined (40°) for most of the time to limit the maximum heat flux. After about 960 s the angle of attack is linearly reduced until a value of 15°, achieved at t = 1250 s, and kept constant.

HORUS flies an equilibrium-glide trajectory, i.e., its flight-path angle changes only very little over time. Since the chosen angle of attack implies a large lift force, the vehicle requires a large bank angle to prevent it from skipping and to keep it flying an equilibrium-glide trajectory. The bank angle can be modulated between -89 and 89 degrees. Moreover, to remain flying towards the target, HORUS performs a number of bank reversals, during which the sign of the bank angle is instantaneously flipped.

**Table 1. Main characteristics of HORUS' reference mission.**[33]

| Property | Value | Property | Value |
|---|---|---|---|
| Wing area ($S_{ref}$) [m$^2$] | 110 | Maximum heat flux [kW/m$^2$] | 530 |
| Reentry mass [kg] | 26029 | Maximum g-load [-] | 2.5 |
| Nose Radius [m] | 0.8 | Maximum dynamic pressure [N/m$^2$] | $1{\cdot}10^4$ |
| Initial altitude [km] | 122 | Terminal altitude [km] | $25 \pm 2$ |
| Initial longitude [°] | -106.7 | Terminal Mach number [-] | $2.5 \pm 0.5$ |
| Initial latitude [°] | -22.3 | Terminal distance [km] | $\pm 2$ |
| Initial velocity [m/s] | 7435.5 | Runway longitude [°] | -53.0 |
| Initial flight-path angle [°] | -1.43 | Runway latitude [°] | 5.0 |
| Initial heading [°] | 70.75 | | |

## B. Environmental and Aerodynamic Models

Here, the models for the shape, gravity field and atmosphere of the Earth are listed. Note that only analytical functions can be transformed into recurrence relations, so all data tables will be fit with analytical functions.

*Gravity model with $J_2$ term*

A more accurate approximation of the gravity field can be obtained if we model better the mass distribution of the Earth. Mathematically, the oblateness of the Earth can be taken into account with the introduction of the zonal harmonic $J_2$. This correction depends on the radius and the geodetic latitude $\phi$, and can be expressed as

$$g(r,\phi) = \frac{\mu_\oplus}{r^2} \cdot \left[1 + \frac{3}{2} \cdot J_2 \cdot \left(\frac{r}{R_\oplus}\right)^2 \left(1 - 3\sin^2\phi\right)\right] \tag{28}$$

where the gravitational parameter of the Earth $\mu_\oplus$ is equal to $3986004.418 \cdot 10^8$ km$^3$/s$^2$, the zonal coefficient $J_2$ is $1.0826271 \cdot 10^{-3}$, while the semi-major axis $R_\oplus$ is considered equal to 6378.137 m. Further zonal coefficients can be neglected, as for the mission proposed here, no significant differences were observed w.r.t. approximations having higher order-degree harmonic coefficients (e.g., as in the case of the WGS84[34]).

*Atmosphere*

For the atmosphere modeling, an exponential profile is used[7]

$$\rho = \rho_0 e^{-h/h_s} \tag{29}$$

where $\rho_0$ is equal to 1.2256 kg/m$^3$, and $h_s$ is the height scale, equal to 7200 m. The temperature model should be theoretically consistent with the model describing the density and the pressure. That is the isothermal model. However the temperature is often approximated by the junction of a series of piecewise affine functions. Indeed, for each altitude, it can be computed as[35]

$$T(h) = T_{i1} + T_{h,i1}(h - h_{i1}), \quad h \in [h_{i1},\ h_i] \tag{30}$$

and the Mach number can be computed as

$$M = \frac{V}{\gamma_{air} R_{air} T} \tag{31}$$

where $\gamma_{air}$ is the specific heat ratio for the air, equal to 1.4, and $R_{air}$ is the specific air constant, equal to 287.058 J / (kg K).

*Aerodynamics*

The aerodynamics coefficients of HORUS can be computed as follows[36]

$$\begin{aligned} C_{D,trim} = {} & a_{D,0} + a_{D,1}\alpha + a_{D,2}\alpha^2 + a_{D,3}\alpha^3 + a_{D,4}M + a_{D,5}M^2 \\ & + a_{D,6}\alpha M + a_{D,7}\frac{\alpha}{M} + a_{D,8}\frac{\alpha^2}{M} + a_{D,9}\frac{\alpha}{M^2} \end{aligned} \tag{32}$$

$$\begin{aligned} C_{L,trim} = {} & a_{L,0} + a_{L,1}M + \frac{a_{L,2}}{M + a_{L,3}} + \left(a_{L,4} + \frac{a_{L,5}}{M + a_{L,6}}\right) \sin\left(a_{L,7}\alpha + \frac{a_{L,8}\alpha}{M + a_{L,9}}\right) \\ & + \left(a_{L,10} + a_{L,11}M + \frac{a_{L,12}}{M + a_{L,13}}\right) \cos\left(a_{L,7}\alpha + \frac{a_{L,8}\alpha}{M + a_{L,9}}\right) \end{aligned} \tag{33}$$

The coefficients $a_{D,i}$ and $a_{L,i}$ can be found in the work of Bergsma and Mooij.[36]

### C. Trajectory Constraints

In this research, three different trajectory constraints are used. The first is the convective heat flux, given by[37]

$$\dot{Q}_c = \frac{C_1}{\sqrt{R_N}} \sqrt{\rho} V^m \leq 5.3 \cdot 10^5 \text{ W/m}^2 \tag{34}$$

with $R_N$, $C_1$ and $m$ equal to 0.8 m, $5.28137 \cdot 10^{-5}$ Js$^{2.15}$/kg$^{0.5}$/m$^{2.15}$ and 3.15, respectively. The second constraint is the normal load factor,

$$n_z = \frac{|L\cos\alpha + D\sin\alpha|}{g_0} \leq 2.5 \tag{35}$$

while the last constraint is the dynamic pressure.

$$q = \frac{1}{2}\rho V^2 \leq 10^4 \text{ N/m}^2 \tag{36}$$

The mission and the scenario are therefore completely characterized, and is possible to analyze the drag-dynamics.

# V. Drag-Energy Dynamics

In this section the drag-energy dynamics will be derived. The results are not restricted to classical hypotheses such as the use of exponential atmospheric density or constant aerodynamic coefficients. All the contributions coming from the environment and the aerodynamics will be analyzed. The relationships will be used to extract the longitudinal states from the drag-energy solution obtained with the method described in Sec. VI.

## A. Longitudinal equations of motion

Let us consider the longitudinal equations of motion with respect to the energy.[7,38] If we neglect the rotation of the Earth, we get

$$\begin{aligned} h' &= -\frac{\sin\gamma}{D} \\ V' &= \frac{1}{V} + \frac{g}{DV}\sin\gamma \\ \gamma' &= \frac{\cos\gamma}{V^2}\left(g - \frac{V^2}{r}\right)\frac{1}{D} - \frac{1}{V^2}u \end{aligned} \tag{37}$$

where the control u is defined as

$$u = \frac{L}{D}\cos\sigma \tag{38}$$

and $\sigma$ is the bank angle. The independent variable is the specific energy, $E = \frac{V^2}{2} - \left(\frac{\mu_\oplus}{r}\right)$, and the energy dissipation can be expressed as

$$\dot{E} = -DV \tag{39}$$

We are interested to develop a guidance system able to generate feasible solutions in the drag - energy domain. In a similar fashion to what has been done in literature,[1,3,15] we can use a feedback-linearization technique, which allows us to control the second derivative of $D$ with the control $u$. The drag-dynamics will be expressed as a second-second-order system. Let us now differentiate the drag acceleration w.r.t. energy.

$$\begin{aligned} D &= \frac{1}{2}\rho V^2 \frac{S}{m} C_D \\ D' &= D\left(\frac{\rho'}{\rho} + 2\frac{V'}{V} + \frac{{C_D}'}{C_D}\right) \end{aligned} \tag{40}$$

For the second derivative, we get

$$D'' = D'\left(\frac{\rho'}{\rho} + 2\frac{V'}{V} + \frac{{C_D}'}{C_D}\right) + D\left(\frac{\rho''}{\rho} - \frac{\rho'^2}{\rho^2} + 2\frac{V''}{V} - 2\frac{V'^2}{V^2} + \frac{C_D''}{C_D} - \frac{{C_D'}^2}{C_D^2}\right) \tag{41}$$

From the analysis of Eq. (41), we can see that we need some other derivatives as well. In the next sections, each of the contributions will be derived. Specifically, these contributions involve the atmospheric density, the aerodynamic coefficients, the Mach number, and the angle of attack.

## B. Atmospheric density

Equation (41) requires the computation of the derivative of the atmospheric density w.r.t. energy, which can be computed as

$$\begin{aligned} \rho' &= \rho_h h' \\ \rho'' &= \rho_{hh} h'^2 + \rho_h h'' \end{aligned} \tag{42}$$

where $\rho_h$ and $\rho_{hh}$ are the first and second derivatives of the atmospheric density w.r.t. the altitude, which can come from either an analytical or a numerical model. Therefore, we can write

$$\frac{\rho''}{\rho} - \frac{\rho'^2}{\rho^2} = \frac{\rho_{hh} h'^2 + \rho_h h''}{\rho} - \frac{\rho_h^2 h'^2}{\rho^2} \tag{43}$$

Clearly Eq. (43) can be applied to any atmospheric model depending only on the altitude, and reduces to the model used for the Space Shuttle entry guidance[1] when the hypothesis of exponential atmospheric density is assumed.

### C. Aerodynamics

Equation (41) includes the derivative of the drag coefficient as well. In general, the drag coefficient $C_D$ might depend on the angle of attack $\alpha$, the Mach number $M$, and the altitude $h$. Therefore, its derivatives are

$$\begin{aligned} C_D{}' &= C_{D,\alpha}\alpha' + C_{D,M}M' + C_{D,h}h' \\ C_D{}'' &= C_{D,\alpha\alpha}\alpha'^2 + C_{D,\alpha M}\alpha'M' + C_{D,\alpha h}\alpha'h' + C_{D,\alpha}\alpha'' + \\ &+ C_{D,M\alpha}M'\alpha' + C_{D,MM}M'^2 + C_{D,Mh}M'h' + C_{D,M}M'' + \\ &+ C_{D,h\alpha}h'\alpha' + C_{D,hM}h'M' + C_{D,hh}h'^2 + C_{D,h}h'' \end{aligned} \tag{44}$$

The derivatives $C_{D,i}$ and $C_{D,jk}$ are the first and second derivatives of the drag coefficient w.r.t. the variables $i$, and $j$, $k$, respectively. These terms are computed with central differences.

### D. Mach number

For the Mach number derivatives we can write

$$\begin{aligned} M' &= M_h h' + M_V V' \\ M'' &= M_{hh}h'^2 + 2M_{Vh}h'V' + M_h h'' + M_{VV}V'^2 + M_V V'' \end{aligned} \tag{45}$$

The derivatives of the Mach number w.r.t. $h$ and $V$ can be obtained analytically from the definition of Mach number, $M = V/\sqrt{\gamma_{air}R^*T}$

$$M_h = -\frac{M}{2}\frac{T_h}{T}, \quad M_V = \frac{1}{\sqrt{\gamma_{air}R^*T}} \tag{46}$$

$T_h$ is the temperature derivative w.r.t. the altitude, and can be obtained numerically from the model used. $\gamma_{air}$ is the specific heat ratio of the air, assumed equal to 1.4, and $R^*$ is the specific gas constant for Earth, equal to 287.058 J/kg K.

**Remark 2** The derivatives of the angle of attack $\alpha'$ and $\alpha''$, are known, as the function $\alpha(E)$ is given in numerical form.

### E. Feedback linearized dynamics

With the previous contributions defined, it is now possible to define the feedback-linearized dynamics. Let us define the second derivatives of altitude $h$ and velocity $V$ w.r.t. energy. Starting from Eq. (37), and differentiating twice we get the following expressions.

$$\begin{aligned} h'' &= \frac{\sin\gamma}{D^2}D' - \frac{\cos\gamma}{D}\gamma' \\ V'' &= -\frac{V'}{V^2} + \frac{g'\sin\gamma}{DV} + \frac{g\cos\gamma\gamma'}{DV} - \frac{g\sin\gamma}{D^2V^2}\left(D'V + DV'\right) \end{aligned} \tag{47}$$

Since the required derivatives have been defined, we can build the relationship between the second derivative of drag acceleration $D''$ and the control $u$. To do so, we will express all variables in affine form, separating the part depending on the control, from the part that does not. For the flight-path angle, we have

$$\gamma' = a_\gamma + b_\gamma u \tag{48}$$

with

$$a_\gamma = \frac{\cos\gamma}{D}\left(\frac{g}{V^2} - \frac{1}{r}\right) + C_\gamma, \quad b_\gamma = -\frac{1}{V^2} \tag{49}$$

with $C_\gamma$ representing a correction term coming from the presence of $\omega_\oplus$ in the differential equation of the flight-path angle in Eq. (102), and equal to

$$C_\gamma = -2\frac{\omega_\oplus\cos\phi\sin\psi}{DV} - \frac{\omega_\oplus^2 r\cos\phi}{DV^2}\left(\cos\gamma\cos\phi + \sin\gamma\sin\phi\cos\psi\right), \tag{50}$$

where the profiles for $\phi$ and $\psi$ are obtained by linearly interpolating between their corresponding initial and final values along the trajectory. The second derivative of altitude becomes

$$h'' = a_h + b_h u \tag{51}$$

with

$$a_h = \sin\gamma \frac{D'}{D^2} - \frac{\cos\gamma}{D} a_\gamma, \quad b_h = -\frac{\cos\gamma}{D} b_\gamma \tag{52}$$

The second derivative of atmospheric density becomes

$$\rho'' = a_\rho + b_\rho u \tag{53}$$

with

$$a_\rho = \rho_{hh} h'^2 + \rho_h a_h, \quad b_\rho = \rho_h b_h \tag{54}$$

For the velocity we have

$$V'' = a_V + b_V u \tag{55}$$

with

$$a_V = -\frac{V'}{V^2} + \frac{g' \sin\gamma}{DV} + \frac{g\cos\gamma a_\gamma}{DV} - \frac{g\sin\gamma}{D^2 V^2}\left(D'V + DV'\right), \quad b_V = \frac{g\cos\gamma b_\gamma}{DV} \tag{56}$$

The second derivative of Mach number can be expressed as

$$M'' = a_M + b_M u \tag{57}$$

with

$$a_M = M_{hh} h'^2 + 2M_{Vh} h' v' + M_h a_h + M_{VV} V'^2 + M_V a_V, \quad b_M = M_h b_h + M_V b_V \tag{58}$$

The second derivatives of Mach number are

$$M_{hh} = \frac{3}{4} M \left(\frac{T_h}{T}\right)^2 - \frac{M}{2}\frac{T_{hh}}{T}, \quad M_{hV} = M_{Vh} = -\frac{1}{2}\frac{T_h}{T} \tag{59}$$

and $M_{VV} = 0$. Finally, for the second derivative of $C_D$, we have

$$C_D'' = a_{C_D} + b_{C_D} u \tag{60}$$

with

$$\begin{aligned} a_{C_D} &= C_{D,\alpha\alpha}\alpha'^2 + C_{D,\alpha M}\alpha' M' + C_{D,\alpha h}\alpha' h' + C_{D,\alpha}\alpha'' + \\ &+ C_{D,M\alpha} M'\alpha' + C_{D,MM} M'^2 + C_{D,Mh} M' h' + C_{D,M} a_M + \\ &+ C_{D,h\alpha} h'\alpha' + C_{D,hM} h' M' + C_{D,hh} h'^2 + C_{D,h} a_h \\ b_{C_D} &= C_{D,M} b_M + C_{D,h} b_h \end{aligned} \tag{61}$$

The second derivative of drag acceleration can thus be expressed as

$$D'' = a_D + b_D u \tag{62}$$

with

$$\begin{aligned} a_D &= D'\left(\frac{\rho'}{\rho} + 2\frac{V'}{V} + \frac{C_D{}'}{C_D}\right) + D\left(\frac{a_\rho}{\rho} - \frac{\rho'^2}{\rho^2} + 2\frac{a_V}{V} - 2\frac{V'^2}{V^2} + \frac{a_{C_D}}{C_D} - \frac{C_D{}^2}{C_D^2}\right) \\ b_D &= D\left(\frac{b_\rho}{\rho} + 2\frac{b_V}{V} + \frac{b_{C_D}}{C_D}\right) \end{aligned} \tag{63}$$

We can now design the guidance scheme based on the pseudospectral convex scheme.

## VI. Convexification of drag-energy guidance problem

In this section the drag-energy problem in pseudospectral convex form will be formulated. The first step is the proper computation of the drag-energy feasible space. After that it is possible to formulate the problem to be solved, first in general form, and then in the frame of the proposed pseudospectral convex method.

### A. Drag-energy feasible space

The first operation to perform is the determination of the feasible drag-energy space. By feasible space in this context we mean those points on the drag-energy plane, which do not cause any constraint violation, (e.g., a too large load factor or heat-flux). In fact, one can observe that, in the hypothesis of nominal angle of attack, $\alpha = \alpha(E)$, all the constraints are a function of altitude and velocity only. $E$ is the specific mechanical energy of the system, equal to $\frac{V^2}{2} - \frac{\mu_\oplus}{r}$, and is a function of altitude and velocity, too, while $\mu_\oplus$ is the Earth gravitational parameter. Therefore, for each of the constraints, and each energy level, we can solve a system of two nonlinear equations, obtaining the altitude and velocity, which generate the maximum value of a specific constraint. Since $\alpha$ is a given function of energy, we can compute the corresponding drag acceleration. If we exceed that specific value at that energy level, the specific constraint will be violated. This process can be done for each of the three constraints considered here, and is performed by using the bisection method to solve the systems of nonlinear equations.

*Dynamic pressure*

In this case, for each value of the energy $E$, the two equations to be solved are

$$\begin{aligned} \frac{V^2}{2} - \frac{\mu_\oplus}{h + r_\oplus} &= E \\ \frac{1}{2}\rho(h)V^2 &= \bar{q}_U \end{aligned} \tag{64}$$

where $q_U$ is the maximum value allowed for the dynamic pressure. The solution to Eq. (64) will give us the altitude $h_q$ and velocity $V_q$ profiles, which maximize the dynamic pressure. The corresponding drag acceleration is

$$D_{\bar{q},max} = \frac{1}{2}\rho(h_q){V_q}^2\frac{S}{m}C_D(\alpha, h_q, V_q) \tag{65}$$

*Heat flux*

In this case the two equations to be solved are

$$\begin{aligned} \frac{V^2}{2} - \frac{\mu_\oplus}{h + r_\oplus} &= E \\ \frac{C_1}{\sqrt{R_N}}\sqrt{\rho}V^m &= \dot{Q}_U \end{aligned} \tag{66}$$

where $\dot{Q}_U$ is the maximum value allowed for the heat-flux. In this case the solution to Eq. (66) will give us the altitude $h_Q$ and velocity $V_Q$ profiles which maximize the heat flux. The corresponding drag acceleration is

$$D_{\dot{Q},max} = \frac{1}{2}\rho(h_Q){V_Q}^2\frac{S}{m}C_D(\alpha, h_Q, V_Q) \tag{67}$$

*Vertical load factor*

The third constraint taken into account is the vertical load factor. The corresponding equations to be solved are

$$\begin{aligned} \frac{V^2}{2} - \frac{\mu_\oplus}{h + r_\oplus} &= E \\ \frac{|L(\alpha, h, V)\cos\alpha + D(\alpha, h, V)\sin\alpha|}{g_0} &= n_{z,U} \end{aligned} \tag{68}$$

where $n_{z,U}$ is the maximum value allowed for the vertical load factor, $L$ and $D$ are the lift and drag accelerations, respectively, and $g_0$ is the gravity acceleration at sea level. In this case the solution to Eq. (68) will give us the altitude $h_{n_z}$ and velocity $V_{n_z}$ profiles, which maximize the vertical load factor. The corresponding drag acceleration is

$$D_{n_z,max} = \frac{1}{2}\rho(h_{n_z}){V_{n_z}}^2\frac{S}{m}C_D(\alpha, h_{n_z}, V_{n_z}) \tag{69}$$

Note that no restrictions on the atmospheric model have been formulated. Therefore, Eqs. (64), (66), and (68) are completely generic.

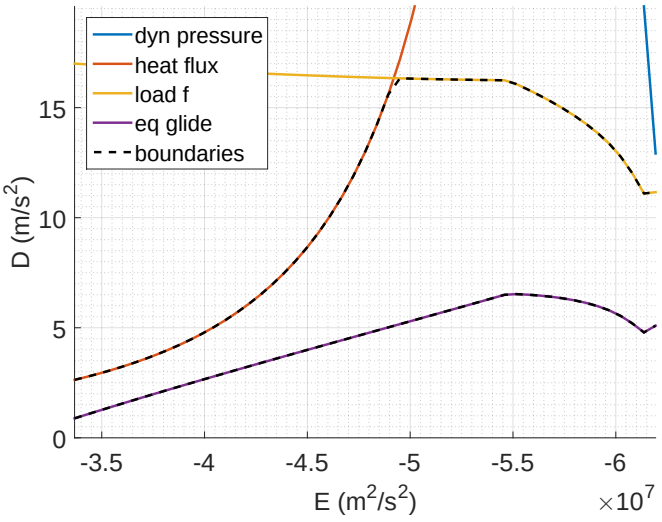


**Figure 3. Drag-energy feasible space obtained for HORUS.**

The drag reference profile to be generated needs to be defined between the upper and the lower boundaries depicted in Fig. 3. We can observe that in the first phase of the atmospheric entry the limiting factor is the heat flux, which grows proportionally to $V^{3.15}$. Once that the aerodynamic accelerations become more relevant and the speed decreases as some energy has been dissipated, the load factor becomes the prominent factor. For this specific mission profile the less demanding constraint is the dynamic pressure, as one can see. Finally, the equilibrium-glide condition provides the minimum level of drag to be generated.

## B. Drag-energy guidance problem

We can now state the drag-energy guidance problem as follows: we want to compute a profile $D = D(E)$, such that

$$D_{min} = D_{Eq_g} \leq D(E) \leq D_{max} = \min \begin{cases} D_{\bar{q},max} \\ D_{\dot{Q},max} \\ D_{n_z,max} \end{cases} \tag{70}$$

Moreover, another constraint comes from the downrange requirements. In fact, one can show that the range traveled by a vehicle can be approximated by[38]

$$R \cong -\int_{E_0}^{E_f} \frac{dE}{D} \tag{71}$$

Initial conditions for the drag value come from the initial conditions of altitude and velocity.

$$D(E_0) = \frac{1}{2}\rho(h_0)V_0^2\frac{S}{m}C_D \tag{72}$$

Moreover, the initial condition of the drag derivative with respect to the energy is a direct consequence of the initial flight-path angle $\gamma(E_0)$. In fact, one can write

$$D'(E_0) = a_{D,\gamma} + b_{D,\gamma}\sin\gamma \tag{73}$$

where $a_{D,\gamma}$ and $b_{D,\gamma}$ can be computed by combining Eqs. (37), (40) and (44).

$$\begin{aligned} a_{D,\gamma} &= D\left[\frac{2}{V^2} + \frac{1}{C_D}\left(C_{D,\alpha}\alpha' + \frac{C_{D,M}M_V}{V}\right)\right] \\ b_{D,\gamma} &= D\left[-\frac{1}{D}\left(\frac{\rho_h}{\rho} + M_h\frac{C_{D,M}}{C_D}\right) + \frac{g}{DV}\left(\frac{2}{V} + \frac{C_{D,M}M_V}{C_D}\right)\right] \end{aligned} \tag{74}$$

Note that the same conditions can be applied to the final values of $D$ and $D'$ if corresponding values of $h$, $V$ and $\gamma$ at the end of the mission are assigned. Finally, a common assumption in drag-energy guidance methods for atmospheric entry is to assume the second derivative of the drag acceleration, given by Eqs. (62) and (63), equal to 0. Therefore, it is meaningful to include it in the problem as variable to be minimized, such that the resulting trajectories will tend to a quasi-gliding solution. The problem can be stated as follows. We are interested to compute drag-energy profiles such that

$$J = D'' = a_D + b_D u \tag{75}$$

is minimized while Eqs. (70)-(74) are satisfied. This choice will generate a drag profile which does not evolve too abruptly, leading to smoother longitudinal states. This problem can be discretized by using LPM introduced in Sec. II. Pseudospectral methods provide the linear operators to approximate first and second derivatives w.r.t. the energy through Eqs. (10) and (14). This means that we can transcribe the previous problem as follows: let us define the discrete values of drag acceleration as

$$\mathbf{X} = \left\{ \begin{array}{c} X_0 \\ X_1 \\ \vdots \\ X_n \end{array} \right\} \tag{76}$$

We can now define the problem in discrete Lobatto form as

$$\text{minimize} \;\; D'' = \text{minimize} \;\; \left\| \mathbf{D}_{Lb}^2 \mathbf{X} \right\|_2 \tag{77}$$

subject to

$$D_{min} \leq X_i \leq D_{max} \quad i \in [0, \dots n] \tag{78}$$

and

$$X_0 = D_0, \quad X_0' = D_0' \tag{79}$$

To impose the range to be flown, we can use Eq. (16), and write

$$R \cong -\int_{E_0}^{E_f} \frac{dE}{D} = -\frac{E_f - E_0}{2} \sum_{i=0}^{n} \frac{w_i}{X_i} \tag{80}$$

Moreover, further constraints might be added at the end of the mission as

$$X_n = D_f, \quad X_n' = D_f' \tag{81}$$

The problem represented by Eqs. (77)-(81) is completely transcribed in Lobatto pseudospectral form. Unfortunately, it is not a convex problem, as we have a nonlinear equality constraint, given by Eq. (80), and therefore convex programming cannot be applied to the problem in this form. To overcome this difficulty the following observations were made.

- The only non-convex constraint is a linear combination of the inverses of the variables $X_i$, $i \in [0, \dots n]$
- All other constraints are boundary constraints, except the minimization of the second derivative with respect to energy

Let us introduce a new set of variables $I_i$, defined as

$$I_i = \frac{1}{X_i} \quad i = [0, \dots n] \tag{82}$$

We can reformulate all the constraints by using this new definition. The first, and most important consequence is that the non-convex equality constraint becomes a linear equality relationship, which, in fact, can be imposed as convex constraint.

$$R = -\frac{E_f - E_0}{2} \sum_{i=0}^{n} w_i I_i \quad i \in [0, \dots n] \tag{83}$$

Concerning the other constraints we can use Eq. (82) and rewrite them taking this transformation into account. Therefore, Eq. (79) becomes

$$I_0 = \frac{1}{D_0}, \quad I_0' = -\frac{2D_0'}{D_0^2} \tag{84}$$

Equivalently, Eq. (81) is expressed as

$$I_n = \frac{1}{D_f}, \quad I_n' = -\frac{2D_f'}{D_f^2} \tag{85}$$

The upper and lower boundaries expressed by Eq. (78) become now

$$D_{max} = I_{min} \leq I_i \leq I_{max} = D_{min}, \quad i \in [0, \dots n] \tag{86}$$

Finally, we need to transform the cost function. If we invert Eq. (82), that is

$$X(E) = \frac{1}{I(E)} \tag{87}$$

and differentiate twice we get

$$X'' = \frac{2(I')^2}{I^3} - \frac{I''}{I^2} \tag{88}$$

which means that

$$\|X''\|_2 = \left\| \frac{2(I')^2}{I^3} - \frac{I''}{I^2} \right\|_2 \tag{89}$$

Since $I$ always assumes finite, positive values, we can approximately minimize $\|X''\|_2$ by minimizing the single contributions, that is,

$$\min \|X''\|_2 \Longleftarrow \begin{cases} \min \|I'\|_2 \\ \min \|(I'')\|_2 \end{cases} \tag{90}$$

We can therefore include two slack variables $s' > 0$ and $s'' > 0$ such that

$$\begin{aligned} \|I'\|_2 &= \left\|\mathbf{D}_{Lb}^1 \mathbf{I}\right\|_2 \leq s' \\ \|I''\|_2 &= \left\|\mathbf{D}_{Lb}^2 \mathbf{I}\right\|_2 \leq s'' \end{aligned} \tag{91}$$

and rewrite the cost function as

$$\text{minimize} \;\; J = s' + s'' \tag{92}$$

**Remark 3** Note that the approximation taken in this approach is given by the fact that the values of $I$, which appears in the denominator of Eq. (89) are not taken into account. However, we know that $I$ is always positive; therefore, if $I'$ and $I''$ tend to 0, $X''$ tends to 0 as well.

Equations (83)-(92) completely define the drag-energy guidance problem, which can be solved as a standard SOCP problem. Throughout this work ECOS[32] has been used. The resulting drag-energy profile is depicted in Fig. 4. It is possible to observe that all the constraints are satisfied. The profile is smooth, and defined between $D_{min}$ and $D_{max}$. Moreover, conditions on the initial drag value and the drag derivative are also satisfied, as the generated profile perfectly matches with the values at the end of the pre-guidance phase, represented in the plot by the green profile. All the constraints are satisfied too. Moreover, the second derivative of the drag acceleration is minimized, as expected, excepted in the initial value, that is constrained by the initial bank angle.

### C. States extraction

Once that the drag-energy profile has been computed, we can extract the longitudinal states and the bank angle which satisfy the associated drag dynamics. For each value on the drag-energy plane belonging to the

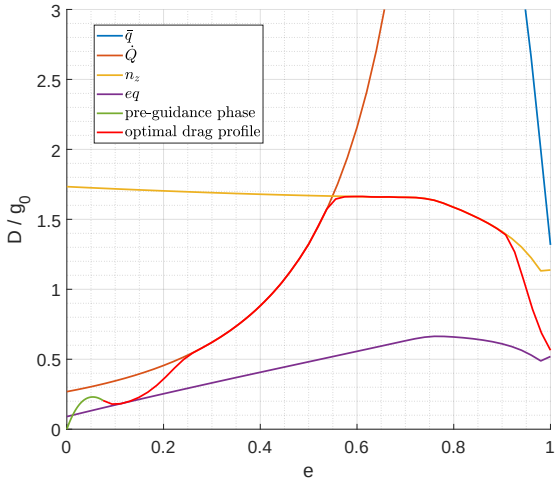


**Figure 4. Reference drag profile obtained via pseudospectral convex optimization.**

solution we can extract the corresponding altitude and speed by numerically solving the following set of two equations

$$\begin{aligned} E &= \frac{V^{*2}}{2} - \frac{\mu_\oplus}{h^* + r_\oplus} \\ D &= \frac{1}{2}\rho(h^*)V^{*2}\frac{S}{m}C_D \end{aligned} \tag{93}$$

The flight-path angle can be computed by inverting Eq. (73)

$$\gamma = \sin^{-1}\left(\frac{D' - a_{D,\gamma}}{b_{D,\gamma}}\right) \tag{94}$$

Finally, Eq. (63) can be inverted to extract the bank angle. First, the feedforward vertical control can be computed as

$$u_{FF} = \frac{D'' - a_D}{b_D} \tag{95}$$

and the bank angle is

$$\sigma = \cos^{-1}\left(\frac{u_{FF}}{C_L/C_D}\right) \tag{96}$$

Results are depicted in Fig. 5 The extracted states satisfy the constraints defined in Table 1, and are consistent with the solution obtained in previous researches for the same scenario.[36] The bank angle is initially very large and decreases continuously, as expected.

### D. Feedback Guidance

We can complete the guidance law by integrating a feedback term in the scheme. In a similar fashion to what has been done in literature,[39] let us define the drag error and its derivatives,

$$\begin{aligned} \Delta D &= D - D_{ref} \\ \Delta D' &= D' - D'_{ref} \\ \Delta D'' &= D'' - D''_{ref} \end{aligned} \tag{97}$$

where the subscript $ref$ refers to the reference solution obtained by using the method described in Sec. VI. The objective is to obtain a combined feedforward-feedback control law:

$$u = u_{FF} + u_{FB} \tag{98}$$

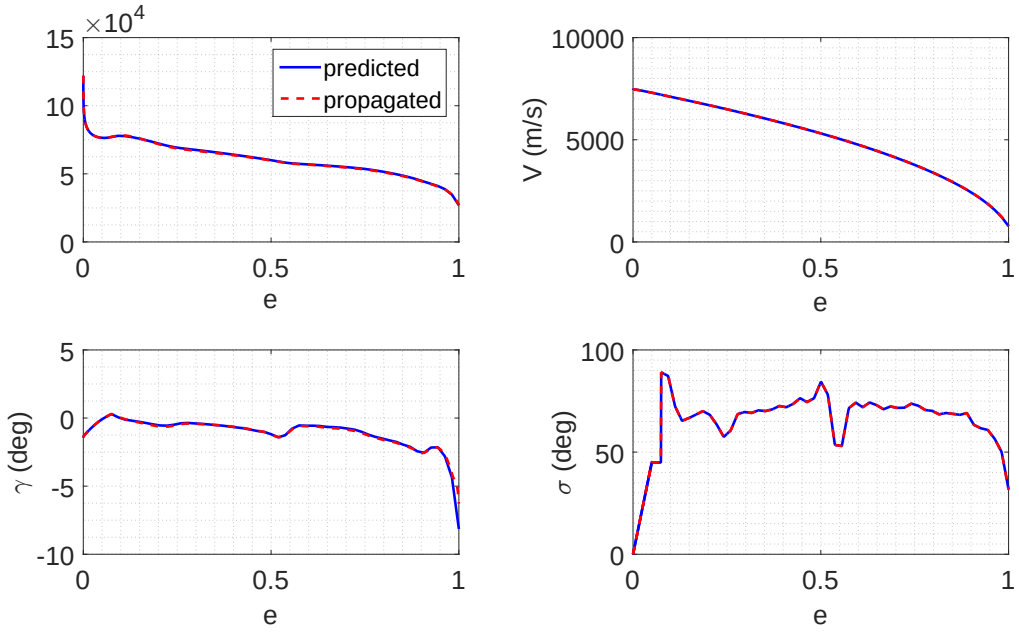


**Figure 5. Longitudinal states and bank angle extracted from drag-energy profile, compared with corresponding open-loop propagation.**

where the first term of the right side of Eq. (98) is given by Eq. (95). We need to determine now $u_{FB}$. Specifically we are interested to model the error dynamics as a second-order system, that is

$$\Delta D'' + 2\zeta_D \omega_D \Delta D' + \omega_D^2 \Delta D + k_D^i \int_{E_0}^{E_F} \Delta D dE = 0 \tag{99}$$

If we solve for the control $u$, we will obtain

$$u = \frac{D''_{ref} - a_D - 2\zeta_D \omega_D \Delta D' - \omega_D^2 \Delta D - k_D^i \int_{E_0}^{E_F} \Delta D dE}{b_D} \tag{100}$$

If we combine Eqs. (96), (98), and (100) we can finally complete the optimal guidance scheme for Horus.

$$u = u_{FF} + \frac{-2\zeta_D \omega_D \Delta D' - \omega_D^2 \Delta D - k_D^i \int_{E_0}^{E_F} \Delta D dE}{b_D} \tag{101}$$

The terms $a_D$, and $b_D$ can be computed with Eq. (63). The damping ratio $\zeta_D$ and the pseudofrequency $\omega_D$ are chosen as a compromise between the saturation of the controls, and the tolerated errors, while the integral term is included to improve the steady-state response of the system. The term pseudofrequency refers to the fact that we are not really dealing with a frequency (having units in Hz), but with something which is only a frequency from the mathematical point of vew, but is physically not, as the independent domain is energy. Therefore, the pseudofrequency is a parameter expressed in $s^2/m^2$. Moreover, since the energy domain is decreasing, to make the system stable, we need to impose eigenvalues with positive real part. This implies that the damping ratio has to assume negative values. Finally, the sign of the bank angle can be computed by using a standard bank-reversal logic.[1,36]

## VII. Numerical Simulations

In this section the equations of motion used for modeling the atmospheric entry are described. The motion is described in terms of altitude $h$, longitude $\theta$, latitude $\phi$, speed $V$, flight-path angle $\gamma$ and velocity azimuth angle $\psi$, equal to zero when the vehicle flies towards north.

$$
\begin{aligned}
\dot{h} &= V \sin\gamma \\
\dot{\theta} &= \frac{V\cos\gamma\sin\psi}{r\cos\phi} \\
\dot{\phi} &= \frac{V\cos\gamma\cos\psi}{r} \\
\dot{V} &= -D - g\sin\gamma + \omega_{\oplus}^2 r\cos\phi\,(\sin\gamma\cos\phi - \cos\gamma\sin\phi\cos\psi) \\
\dot{\gamma} &= \frac{L\cos\sigma}{V} + \left(\frac{V}{r} - \frac{g}{V}\right)\cos\gamma + 2\omega_{\oplus}\cos\phi\sin\psi + \\
&\quad + \frac{\omega_{\oplus}^2 r}{V}\cos\phi\,(\cos\gamma\cos\phi + \sin\gamma\sin\phi\cos\psi) \\
\dot{\psi} &= \frac{L\sin\sigma}{V\cos\gamma} + \frac{V}{r}\cos\gamma\sin\psi\tan\phi + 2\omega_{\oplus}\,(\sin\phi - \cos\phi\tan\gamma\cos\psi) + \\
&\quad + \frac{\omega_{\oplus}^2 r}{V\cos\gamma}\sin\phi\cos\phi\sin\psi
\end{aligned}
\tag{102}
$$

The model represented by Eq. (102) has as an indirect control input the angle of attack $\alpha$ (if it can be modulated), which affects $C_L$ and $C_D$, and as direct control input the bank angle $\sigma$. This model will be used for validation of the proposed method.

### A. Monte-Carlo campaign

In this section we describe the results associated with a Monte-Carlo campaign of 1000 cases. The initial dispersions included in the analysis are described in Table 2. Note that larger dispersions could be handled

**Table 2. Dispersions at the entry interface (uniform distribution).**

| Variable | Dispersion | Units |
|---|---|---|
| $\Delta h$ | $[-250\ 250]$ | m |
| $\Delta\theta$ | $[-0.1\ 0.1]$ | deg |
| $\Delta\phi$ | $[-0.1\ 0.1]$ | deg |
| $\Delta V$ | [-15 15] | m/s |
| $\Delta\gamma$ | [-0.01 0.01] | deg |
| $\Delta\psi$ | [-0.01 0.01] | deg |

by the method itself. However the dispersion is here limited, as the solution could be outside the vehicle's capabilities in terms of heat-flux and / or load factor. For instance, in case the vehicle has to strongly reduce its range-to-go, the larger drag required could be not compatible with the constraints' limits, leading therefore to the infeasibility of problem. In Fig. 6 the longitudinal states obtained as function of the non-dimensional energy $e = \frac{E-E_0}{E_f-E_0}$ are depicted. Altitude and velocity are smooth, and continuously differentiable. We can observe instead *removable* discontinuities in some of the flight-path angle profiles. In other words, it might happen that the flight-path angle obtained with this method is continuous, but not continuously differentiable (i.e., a $\mathbf{C}^0$ function). The bank angle shows instead *essential* discontinuities, that is some jumps in the command values. The reason for this behavior is essentially due to the physical limitation of vertical lift. In fact, since the angle of attack is fixed, there will be a corresponding fixed value of $L/D$ as well. As in many other methods, we compute the component of vertical acceleration $u$, given by Eq. (38), and therefore, if this value exceeds the one associated with bank angle equal to 0, a jump in the bank angle (and the second derivative of drag acceleration) is experienced, which translates into a first-kind discontinuity in terms of flight-path angle (and in terms of first derivative of drag acceleration as well). This behavior appears only in few cases, and is not critical, as in real systems the bank-angle rates are limited, but is the main aspect that will be addressed in the follow-up of this work.

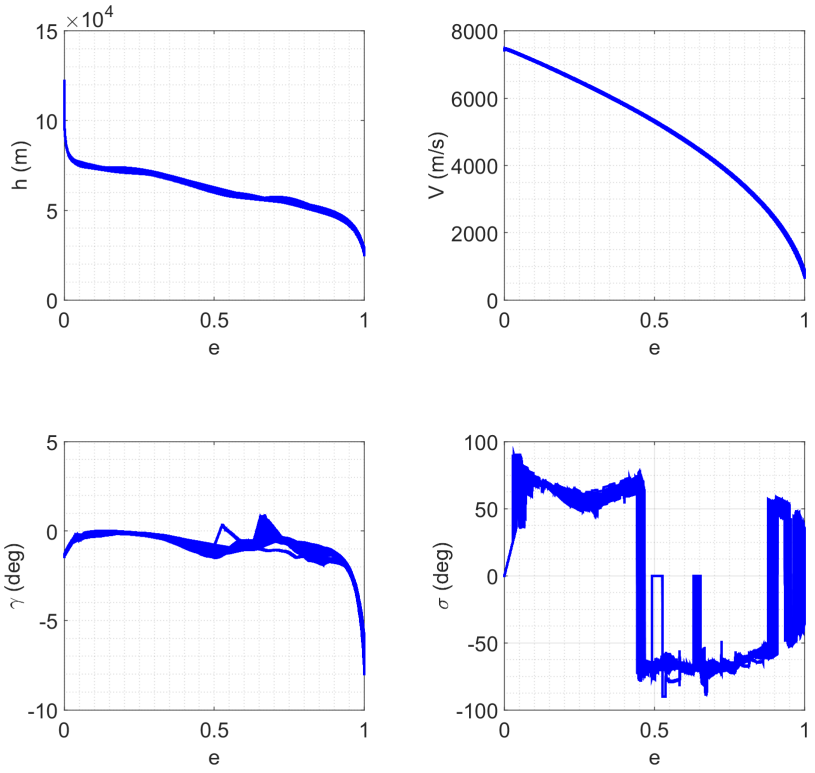


**Figure 6. MC campaign: altitude, speed, flight-path angle, and bank angle.**

Figure 7 shows the constraints, which are indirectly depicted in Fig. 8 as well, in the drag-energy space. All the solutions lie within the feasible constraint space. Specifically, for this scenario the heat-flux and the load factor play a major role in the generation of the constrained trajectory, while the dynamic pressure is less stringent, as for all of the cases this constraint is never active. Finally, Fig. 9 shows the envelope of obtained trajectories, which are all consistent with the scenario. Final dispersions are summarized in Table 3. The mean values of final altitude (169 m), speed (12 m/s) and range-to-go (312 m) are well within the requirements of the scenario. The standard deviations in terms of speed (about 70 m/s) and range-to-go (1.5 km) are within the limits too, although larger than expected.

**Table 3. Final dispersions at the terminal interface.**

| Variable | Dispersion ($1\sigma$) | Units |
|---|---|---|
| $\Delta h$ | $168.6 \pm 1107.3$ | m |
| $\Delta\theta$ | $-0.0036 \pm 0.0055$ | deg |
| $\Delta\phi$ | $-0.0047 \pm 0.0096$ | deg |
| $\Delta V$ | $12.1 \pm 68.95$ | m/s |
| $\Delta R$ | $312.3 \pm 1529.7$ | m |

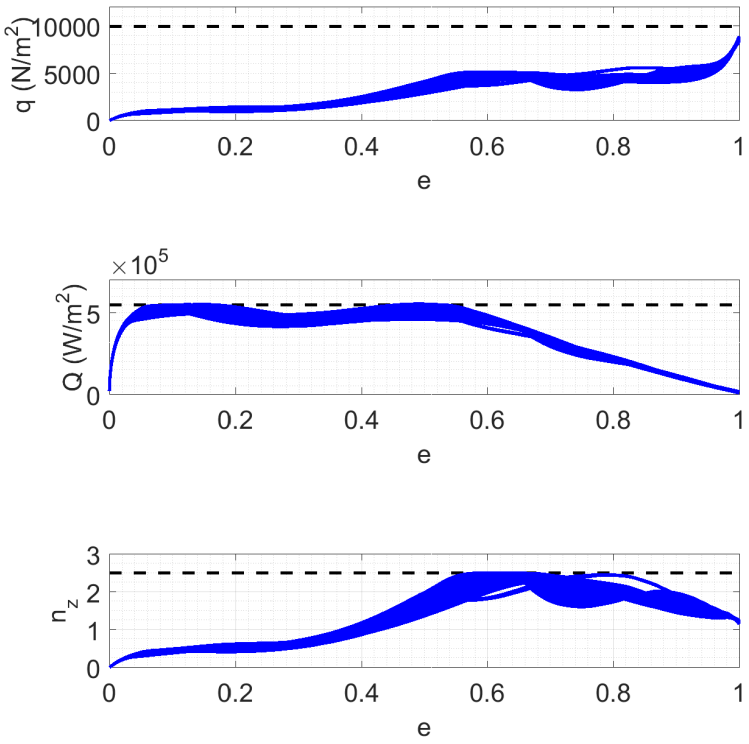


**Figure 7. MC campaign: dynamic pressure, heat flux, and normal load factor.**

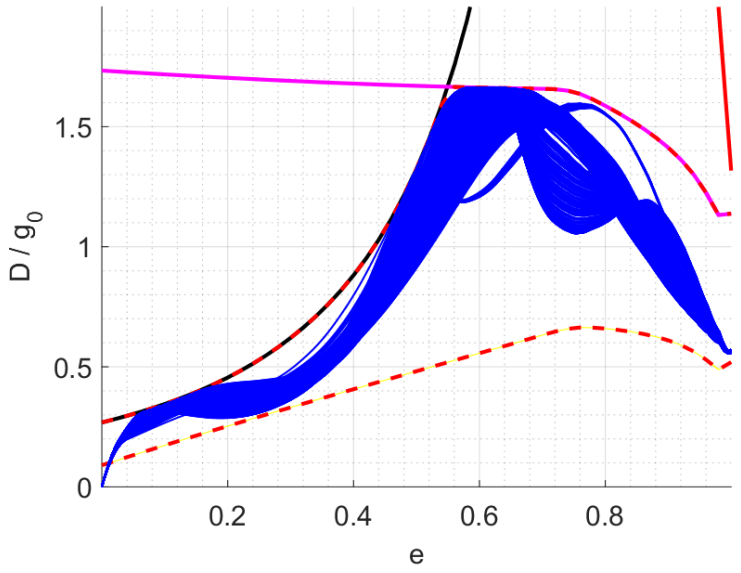


**Figure 8. MC campaign: optimal drag-energy profiles.**

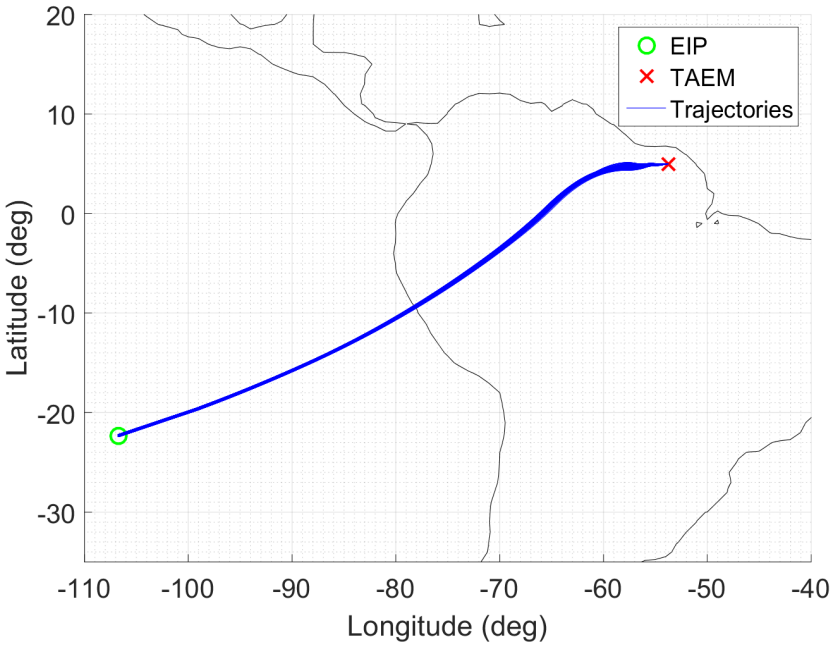


**Figure 9. MC campaign: closed-loop trajectories.**

## VIII. Conclusion and future work

This paper proposes a new strategy for the generation of atmospheric entry guidance solution via convex optimization. The problem is described in terms of drag-energy dynamics, and is not convex because of the nonlinear equality constraint representing the range-to-go condition. The introduction of a new set of variables corresponding to the inverse of drag acceleration allows for a lossless convexification of the problem, and therefore to the possibility to solve it in real-time.

The main difference with respect to the pre-existing literature concerning convex optimization applied to entry guidance problems resides in the fact that here only one convex problem is required to generate a feasible drag-energy profile. The drag profile is later converted into altitude, velocity, flight-path angle and bank angle by exploiting drag-dynamics equations. Moreover, pseudospectral methods are integrated in the proposed strategy to have more accurate differential and integral operators.

The analysis of the results show that the method provides very good results, leading to a mean error in terms of range to go of about 300 m over a total flight distance of more than 6500 km, and an initial dispersion up to $11 \times 10.3$ km$^2$. Most important, the technique enables the capability to recompute the trajectories in real-time, and therefore it is suitable for a potentially high technology readiness level. Future work will include strategies to reduce the discontinuities associated with control saturation, and a comparison with the results obtained by using a more traditional nonlinear programming approach to further assess the quality of the results.

## References

[1]Harpold, J. D. and Graves, C. A., "Shuttle Entry Guidance," *Journal of Astronautical Sciences, Vol.27 No.3, May-June 1979, pp.239-268*, 1979.

[2]Lu, P., "Entry Guidance: A Unified Method," *Journal of Guidance, Control, and Dynamics, Vol.37 No.3, May-June*, 2014.

[3]Mease, K. D., Chen, D. T., Teufel, P., and Schöneberger, H., "Reduced-Order Entry Trajectory Planning for Acceleration Guidance," *Journal of Guidance, Control, and Dynamics, Vol.25 No.2, March-April*, 2002.

[4]Mooij, E., "Adaptive Heat-Flux Tracking for Re-entry Guidance," *AIAA/AAS Astrodynamics Specialist Conference, San Diego, USA*, 2014.

[5]Lu, P., "Entry Guidance and Control for Reusable Launch Vehicles," *AIAA Guidance, Navigation, and Control Conference, San Diego, USA*, 1996.

[6]Tu, K. Y., Munir, M. S., and Mease, K. D., "Drag-Based Predictive Tracking Guidance for Mars Precision Landing," *Journal of Guidance, Control and Dynamics, Vol.23 No. 4, July-August 2000, pp.620-628*, 2000.

[7]Sagliano, M., *Development of a Novel Algorithm for High Performance Reentry Guidance*, Ph.D. thesis, 2016.

[8]Betts, J. T., *Practical Methods for Optimal Control and Estimation Using Nonlinear Programming, $2^{nd}$ ed.*, SIAM, Philadelphia, 2010.

[9]Bollino, K. P., Ross, I. M., and Doman, D., "Optimal Nonlinear Feedback Guidance for Reentry Vehicles," *AIAA Guidance Navigation, and Control Conference and Exhibit, Keystone, USA*, 2006.

[10]Singh, B. and Bhattacharya, R., "Optimal Guidance of Hypersonic Vehicles Using B-Splines and Galerkin Projection," *AIAA Guidance, Navigation and Control Conference and Exhibit*, 2008.

[11]Marwaha, M., Singh, B., Valasek, J., and Bhattacharya, R., "Integrated Guidance and Fault Tolerant Adaptive Control for Mars Entry Vehicle," *AIAA Guidance, Navigation, and Control Conference*, edited by AIAA, Vol. 2009, 2009.

[12]Sagliano, M., Theil, S., Bergsma, M., D'Onofrio, V., Whittle, L., and G., V., "On the Radau Pseudospectral Method: theoretical and implementation advances," *CEAS SPACE Journal*, 2017.

[13]Gill, P. E., Murray, W., and Saunders, M. A., *User's Guide for SNOPT Version 7: Software for Large-Scale Nonlinear Programming*, University of California, San Diego, USA, 2008.

[14]Wächter, A. and Biegler, L. T., "On the implementation of an interior-point filter linesearch algorithm for large-scale nonlinear programming," *Math. Program. 106(1) , Springer-Verlag, New York, 2006*, 2006.

[15]Saraf, A., Leavitt, J. A., Chen, D. T., and Mease, K. D., "Desing and Evaluation of an Acceleration Guidance Algorithm for Entry," *Journal of Spacecraft and Rockets, Vol.41 No.6, November-December*, 2004.

[16]Schierman, J. and Hull, J., "In-Flight Entry Trajectory Optimization for Reusable Launch Vehicles," Guidance, Navigation, and Control and Co-located Conferences, American Institute of Aeronautics and Astronautics, Aug. 2005.

[17]Sagliano, M., Mooij, E., and Theil, S., "Onboard Trajectory Generation for Entry Vehicles via Adaptive Multivariate Pseudospectral Interpolation," *Journal of Guidance, Control, and Dynamics*, Vol. 40, No. 2, sep 2016, pp. 466–476.

[18]Boyd, S. and Vandenberghe, L., *Convex Optimization*, 2004.

[19]Acikmese, B. and Ploen, S. R., "Convex programming approach to powered descent guidance for mars landing," *Journal of Guidance, Control, and Dynamics*, Vol. 30, No. 5, 2007, pp. 1353–1366.

[20]Blackmore, L., Acikmese, B., and Scharf, D. P., "Minimum-Landing-Error Powered-Descent Guidance for Mars Landing Using Convex Optimization," *Journal of Guidance, Control, and Dynamics*, Vol. 33, No. 4, July 2010, pp. 1161–1171.

[21]Sagliano, M., "Pseudospectral Convex Optimization for Powered Descent and Landing," *Journal of Guidance, Control and Dynamics*, 2018.

[22]Huntington, G. T., *Advancement and analysis of a Gauss pseudospectral transcription for optimal control problems*, Ph.D. thesis, Citeseer, 2007.

[23]Mooij, E., *The HORUS-2B Reference Vehicle*, Delft University of Technology. Memorandum M-682, 1995.

[24]Elissar, "Description of DIDO Optimal Control software," June 2015.

[25]Rao, A. V., Benson, D. A., Darby, C. L., Patterson, M. A., Francolin, C., Sanders, I., and Huntington, G. T., "GPOPS: A MATLAB Software for Solving Multiple-Phase Optimal Control Problems Using the Gauss Pseudospectral Method," *ACM Transactions on Mathematical Software*, Vol. 37, No. 2, apr 2010, pp. 1–39.

[26]Fahroo, F. and Ross, I. M., "Direct Trajectory Optimization by a Chebyshev Pseudospectral Method," *Journal of Guidance, Control, and Dynamics*, Vol. 25, No. 1, Jan. 2002, pp. 160–166.

[27]Garg, D., *Advances in Global Pseudospectral Methods for Optimal Control*, Ph.D. thesis, University of Florida, Gainesville, 2011.

[28]Martins, J. R. R., Sturdza, P., and Alonso, J. J., "The Complex-Step Derivative Approximation," *ACM Transactions on Mathematical Software, Vol. 29, No. 3, September 2003, Pages 245262*, 2003.

[29]Abramovitz, M. and Stegun, I. A., *Handbook of Mathematical Functions*, Dover Publications, 1695.

[30]Ben Tal, A. and Nemirovski, A., *Modern Lectures on Convex Optimization*, 2001.

[31]Lobo, M. S., Vandenberghe, L., Boyd, S., and Lebret, H., "Applications of Second-Order Conic Programming," *Linear Algebra and Its Applications*, 1998, pp. 193–228.

[32]Domahidi, A., Chu, E., and Boyd, S., "ECOS: An SOCP Solver for Embedded Systems," *European Control Conference*, 2013.

[33]MBB, "Study on re-entry guidance and control," Tech. Rep. ESA CR (P) 2652, Space Communication and Propulsion Systems Division, 1988.

[34]Department of Defense, "World Geodetic System 1984," Tech. Rep. NIMA TR8350.2 $3^{rd}$ Ed., 1984.

[35]NASA, "U.S. Standard Atmosphere 1976," Tech. Rep. NASA Technical Memorandum X-74335, 1976.

[36]Bergsma, M. C. W. and Mooij, E., "Application of Taylor-Series Integration to Reentry Problems with Wind," *Journal of Guidance, Control, and Dynamics*, Vol. 39, No. 10, Oct. 2016, pp. 2324–2335.

[37]Mooij, E., *Aerospace-Plane Flight Dynamics: Analysis of Guidance and Control Concepts*, Ph.D. thesis, Delft University of Technology, 1998.

[38]Mease, K. D., Chen, D. T., Tandon, S., Young, D. H., and Kim, S., "A Three-Dimensional Predictive Entry Guidance Approach," *AIAA Guidance, Navigation, and Control Conference and Exhibit*, 2000.

[39]Bharadwaj, S., Rao, A. V., and Mease, K. D., "Entry Trajectory Tracking Law via Feedback Linearization," *Journal of Guidance, Control, and Dynamics, Vol.21 No.5, September-October 1998*, 1998.